MOCVD Growth and Characterization of Be-Doped GaN

Benjamin McEwen[1], Michael Reshchikov[2], Emma Rocco[1], Vincent Meyers[1], Kasey Hogan[1], Oleksandr Andrieiev[2], Mykhailo Vorobiov[2], Denis O. Demchenko[2], and Fatemeh Shahedipour-Sandvik[1]*

[1]College of Nanoscale Science and Engineering, SUNY Polytechnic Institute, Albany, New York, 12203-3613, USA

[2]Department of Physics, Virginia Commonwealth University, Richmond, Virginia, 23284-2000, USA

KEYWORDS

III-Nitrides, GaN, Beryllium-doping, *p*-type doping, MOCVD

ABSTRACT

Beryllium has been considered a potential alternative to magnesium as a *p*-type dopant in GaN, but attempts to produce conductive *p*-GaN:Be have not been successful. Photoluminescence studies have repeatedly shown Be to have an acceptor level shallower than Mg, but deep Be defects and other compensating defects render most GaN:Be material n-type or semi-insulating at best. Previous reports use molecular beam epitaxy (MBE) or ion implantation to dope GaN with Be,

almost exclusively. Due the high toxicity of Be organometallics, reports of GaN:Be by metal-organic chemical vapor deposition (MOCVD) has been largely absent. Here, we report a systematic study of growth of GaN:Be by MOCVD. All doped samples show the established UV band and yellow luminescence signature of GaN:Be, and growth conditions resulting in high quality GaN with stable Be incorporation were established. Our results show that the MOCVD growth technique allows for Be incorporation pathways that have not been possible with previous growth methodologies and is highly promising in achieving *p*-type conductivity in GaN:Be.

INTRODUCTION

Over the last three decades, GaN has become an invaluable material for lighting and power management applications[1–14]. Much of the success enjoyed by GaN is due to the realization of *p*-type doping, originally by Amano, et al.[15]. However, despite more than 30 years of development, impurity-doped *p*-type III-Nitrides still suffer from limited carrier concentration and low mobility. Mg, the only widely used and presently viable *p*-type dopant in III-N, is relatively deep, with a level at ~160 meV from the valence band edge in GaN[16]. Because of this, usually only ~1% of Mg dopants are activated acceptors at room temperature, and the high Mg concentration necessary to achieve even moderate hole concentrations can lead to increased impurity scattering and self-compensation by donor-like defects such as V_N[17].

Be has been suggested as an alternative *p*-type dopant, and early results showed promise[18–21]. A shallow defect state was identified in photoluminescence (PL) experiments with a band centered at ~3.38 eV, with an estimated energy level of 118 meV from GaN valence band edge[19]. However, to date, there have been no reliable and repeatable examples of *p*-type GaN:Be. In fact, the majority, if not all, of GaN:Be reported in literature is semi-insulating[22–24], though Ahmad, *et*

al. recently claimed to obtain *p*-type AlN:Be[25]. Recent calculations from first principles predict a deep Be_{Ga} polaronic state, 450–650 meV above the valence band edge, perhaps indicating that highly conductive GaN:Be is impossible to achieve without some novel activation methodologies[26–28]. However, to date, this deep acceptor state has not been found experimentally, and the predicted associated red PL band has never been observed. Recently, Demchenko, *et al.*[29] have explained this phenomenon by calculating the capture cross-sections for the shallow and deep radiative states; the shallow Be_{Ga} state is predicted to be 1–2 orders of magnitude more efficient at capturing photogenerated holes than the deep polaronic state. Nevertheless, while this shallow state is the shallowest acceptor level known in GaN, the exact nature of Be in GaN is not well known.

In light of the promising evidence through first-principles calculations and PL, the substantial challenges standing in the way of GaN:Be development are worth addressing. Aside from one reported Be doped GaN using metal-organic chemical vapor deposition (MOCVD)[30] over a decade ago, no further reporting has been made. While other growth methods such as molecular beam epitaxy (MBE) use effusion cells with a metallic Be source for Be doping, lack of further follow up in MOCVD could be due to the high toxicity of Be-containing compounds for the Be source material, and their resulting difficulty to obtain and utilize. Here, we report on initial results toward the optimization of MOCVD growth conditions to achieve controlled Be incorporation in GaN and high activation efficiency. To the best of the authors' knowledge, no other report exists with a systematic reporting of such development in MOCVD growth of GaN:Be.

EXPERIMENTAL

GaN:Be layers, ~500 nm thick, were grown on unintentionally doped GaN (*u*-GaN, *n*-type) on c-plane sapphire substrates in a vertical cold wall MOCVD reactor. Trimethylgallium (TMGa) and ammonia (NH_3) were used as Ga and N precursors, respectively, with V/III ratio of about 7000. Beryllium acetylacetonate ($Be(acac)_2$) obtained from Strem Chemicals was used as Be precursor (see Supporting Information for SDS). Given the unknown growth space for MOCVD of GaN:Be, several growth conditions were investigated while maintaining TMGa flow at 19 μmol/min, and 970 °C growth temperature, as described in Table 1. For brevity and clarity, we discuss a representative set of three growths marked with "*" in Table 1, for which the $Be(acac)_2$ flow was varied from 460 nmol/min to 3 μmol/min by varying both the $Be(acac)_2$ bubbler temperature and the H_2 carrier gas flow rate. Molar flows of $Be(acac)_2$ were calculated based on vapor pressure values at various temperatures given by Truemper[31]. Immediately after growth, the material was annealed *in situ* under flowing N_2 at 500 Torr and 750 °C for 30 min without removing from the growth chamber. Be concentration in the doped films was determined using dynamic secondary ion mass spectroscopy (SIMS) and surface morphology was characterized using atomic force microscopy (AFM). Characteristic Be-related defects were identified using detailed PL studies. The steady-state PL was excited with a HeCd laser. The as-measured PL spectra were corrected for the spectral response of the PL system, and PL intensity was additionally multiplied by λ^3, where λ is the light wavelength, to present the PL spectra in units proportional to the number of emitted photons as a function of photon energy[32]. Other details of PL experiments can be found elsewhere[32]. Hall effect measurements at room temperature were performed, however the results are inconclusive, pointing to the compensated nature of the material.

Table 1. Growth conditions used for Be doping of GaN thin films. The samples marked with "*" are discussed in greater detail.

Sample ID	Growth Pressure (Torr)	$Be(acac)_2$ Temp. (°C)	Carrier Gas Flow (sccm)	$Be(acac)_2$ Molar Flow (nmol/min)
R0039	300	60	120	3000
R0040*	300	60	120	3000
R0041	300	60	120	3000
R0045*	300	40	120	1400
R0048*	300	40	40	460
R0049	100	20	120	560

RESULTS AND DISCUSSION

From detailed PL studies, which included steady-state and time-resolved PL measured in wide ranges of temperatures and excitation intensities, we concluded that all GaN:Be samples that we studied are semi-insulating. Very intense Be-related yellow band (YL_{Be}) along with the Be-related UVL_{Be} band were observed in all samples. Fig. 1 shows low-temperature PL spectra from the three representative samples. The shape and position of the YL_{Be} band is the same as in Be-doped GaN samples grown by MBE[33]. The characteristic feature of the YL_{Be} band is that its thermal quenching always demonstrates two steps: a small step at about 100 K and an abrupt step at about 200 K[29,34]. This behavior was observed for all samples, and examples are shown in Fig. 2. The quenching in semi-insulating GaN:Be samples always occurs by an abrupt and tunable mechanism[32,35]. Namely, the temperature at which the abrupt quenching of PL begins increases with excitation intensity (the inset to Fig. 2).

The UVL_{Be} band can be recognized by its characteristic shape: a sharp peak at 3.38 eV is followed by several LO phonon replicas the intensities of which correspond to the Huang-Rhys factor of 0.2[29,34]. At T = 18 K, the UVL_{Be} band is caused by electron transitions from the shallow donor to the shallow Be level at 113 meV above the valence band[29], the donor-acceptor-pair (DAP) transitions. With increasing temperature, the DAP-related peaks gradually disappear and a band with a similar shape but shifted by 0.02 eV to higher energies emerges. This new band is caused by electron transitions from the conduction band to the same shallow Be level (eA transitions). The characteristic transformation of the PL spectrum from DAP to eA has previously been observed in MBE-grown GaN:Be samples[29,34] and now in this work in MOCVD-grown samples.

The quantum efficiency of the YL_{Be} band (estimated by comparison with calibrated GaN samples)[32,35] is extremely high and varies from 0.1 to almost 1 in the studied samples. The UVL_{Be} band is less intense, and its quantum efficiency slightly increases with excitation intensity. The same behavior was observed for GaN:Be grown by MBE[34]. The Mg-related UVL_{Mg} band with a peak at 3.27 eV followed by LO phonon replicas was also observed and sometimes obscured the phonon replicas of the UVL_{Be} band. Although the UVL_{Mg} band is relatively strong, it is caused by contamination of Mg with the concentration of $\sim 10^{15}$ cm^{-3} or lower[32].

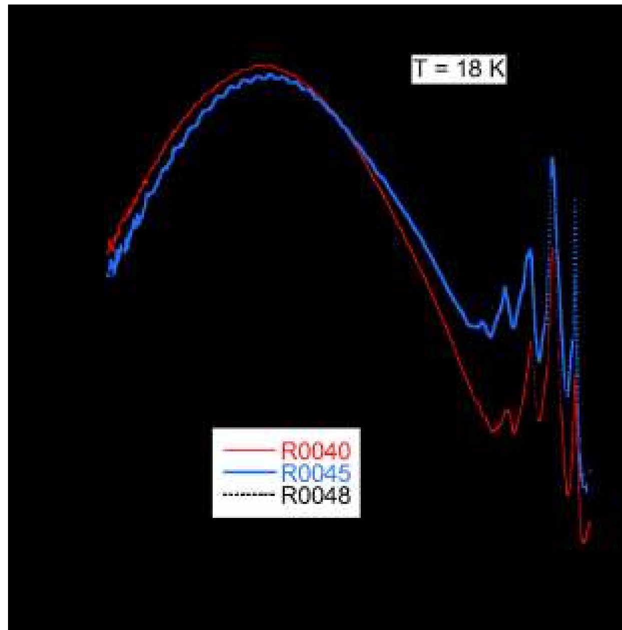

Figure 1. PL spectra of GaN:Be from samples R0040, R0045, and R0048 collected at 18 K with excitation intensity 10^{-4} W/cm^2. The UVL_{Be} peak at 3.38 eV is associated with a shallow acceptor level of Be_{Ga}, and the YL_{Be} band with a maximum at 2.15 eV is presumably caused by a complex defect involving Be_{Ga}. The NBE peak at 3.48 eV is the donor-bound exciton.

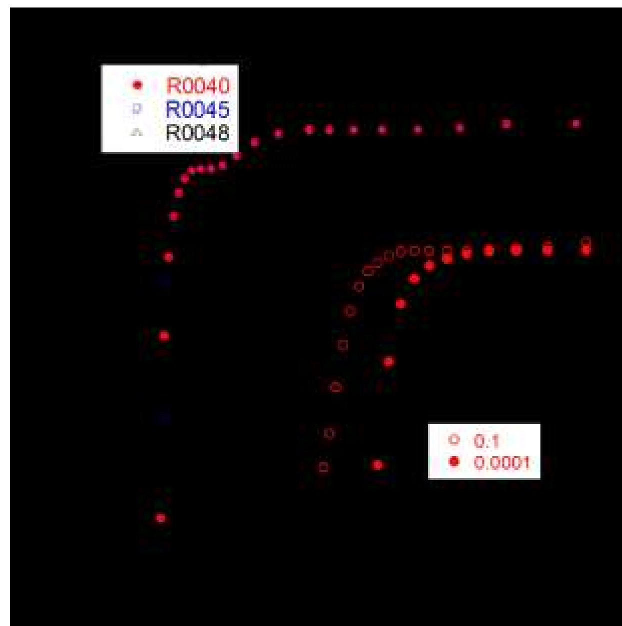

Figure 2. Temperature dependences of the YL_{Be} band intensity at $P_{exc} = 0.0001$ W/cm^2 for R0040, R0045, and R0048 normalized at 18 K. The two-step thermal quenching of the YL_{Be} band confirms the Be-related origin of this band. The inset shows the second step of quenching at two excitation intensities.

The [Be] vs. depth profiles for samples R0040, R0045, and R0048 are plotted in Fig. 3. From R0040 to R0045, the $Be(acac)_2$ flow was reduced from 3000 nmol/min to 1400 nmol/min by reducing the bubbler temperature from 60 °C to 40 °C. The Be concentration profile reveals little if any change in Be incorporation between these two samples, despite >50 % decrease in $Be(acac)_2$ molar flow. In both samples, the [Be] peaks around 5–6×10^{19} cm^{-3} near the surface region and shows a gradual decrease deeper into the doped layer. The high [Be] measured within the nominally undoped GaN region (deeper than ~500 nm) in Fig. 3 is an artifact. To confirm this assumption, SIMS measurements were repeated after removing the top GaN:Be layer (~600 nm) using ICP-RIE, with no discernable Be signal detected in the samples. The cause of the measurement artifact is unknown at this time; however, it may be the result of non-uniform Be incorporation causing the formation of high [Be] domains. Interestingly, despite the presence of oxygen in the $Be(acac)_2$ precursor, uniformly elevated [O] was not observed in doped layers. However, in all doped material, the [O] gradually decreased with depth for the first 200–300 nm down to the bulk [O] value. This long oxygen "tail" was not observed in nominally undoped material. Long surface tails in concentrations of common environmental impurities such as oxygen and carbon are fairly common in SIMS and generally indicate surface contamination in the form of particulate species or an uneven native oxide layer.

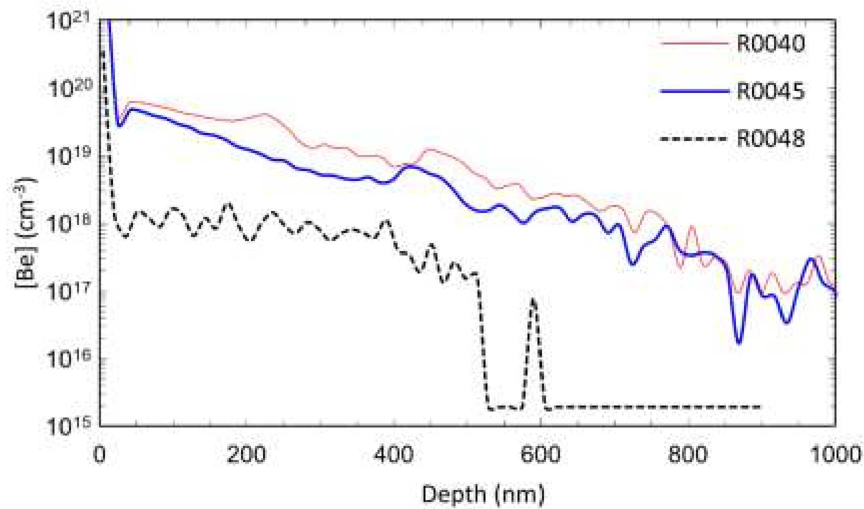

Figure 3. SIMS concentration-depth profiles of Be in R0040, R0045, and R0048.

By decreasing the H_2 carrier gas flow rate from 120 sccm to 40 sccm, the Be(acac)$_2$ molar flow was reduced further to 460 nmol/min for R0048. A decrease in maximum [Be] of over an order of magnitude was measured by SIMS, down to 10^{18} cm^{-3}. Additionally, the incorporation of Be at a lower flow rate appears to result in a more controlled incorporation into the material, with a nearly constant [Be] measured through the depth of the doped layer and a sharp interface between doped and undoped layers. By contrast, the [Be] in R0040 and R0045 decreases through the depth.

It is apparent that at very high Be(acac)$_2$ flow (e.g., R0040, R0045), the [Be] in the GaN saturates, and incorporation efficiency decreases. The non-uniform [Be] concentration through the depth of the doped layer suggests that surface segregation of Be occurs during growth. Surface saturation of Be during growth of GaN:Be using MBE has been reported previously, where [Be] increases during the introduction of Be and peaks at or after Be flux is cut off[20,36,37]. Segregation of other common GaN dopants Si and Mg during MOCVD growth has also been

observed, particularly when doping concentrations exceed the solubility limit[38–41]. Theoretical calculations indicate that steady-state incorporation of the Mg into GaN during growth occurs when the adlayer is populated with ≥0.25 monolayers (ML) of Mg[42,43], and X-ray photoelectron spectroscopy (XPS) measurements have shown surface [Mg] on as-grown GaN:Mg to be much higher than bulk [Mg][39,40]. In addition to dopant accumulation at the surface, lateral inhomogeneity in heavily doped GaN is also common. In particular, Mg, which is electrically similar to Be, is known to segregate into clusters[12,44,45]. It is likely that Be behaves similarly to other dopants in GaN, particularly Mg. Under conditions where $Be(acac)_2$ flow is very high and Be is oversaturated, clusters or second-phase particles of locally high [Be] may form. In the current study, increased $Be(acac)_2$ flow, most probably beyond the point of saturation, results in depression of the intensity of the UVL_{Be} and excitonic PL peaks, further indicating the presence of competing defects and/or degradation of material quality. In contrast, GaN:Be with lower [Be] has higher intensity UVL_{Be} and excitonic peaks, as shown in Fig. 1.

Difficulties with solubility and self-compensation are expected in GaN:Be, owing to the low solubility of Be in GaN and the low formation energies of Be_3N_2 and Be_i^{2+} [18]. The small size of Be exaggerates these effects, but low solubility and self-compensation are well-known issues with Mg in GaN as well. Methods such as using a pulsed growth method (or δ-doping) have been successfully employed in MOCVD GaN:Mg growth to significantly improve Mg incorporation and/or activation efficiency[2,46] and may be effective in GaN:Be. Other methods, such as the use of indium surfactant, have been suggested for improved GaN:Be[47].

AFM scans (Fig. 4) show qualitatively similar surface morphology for R0040 and R0045 with prominent step-bunching. In 10 µm × 10 µm scans, the RMS roughness in R0040 and R0045 is 1.5 nm and 2.3 nm, respectively. In addition to lower [Be] and more controlled Be incorporation,

R0048 had a significantly smoother surface with step bunching significantly suppressed, as shown in Fig. 5 and RMS roughness is <0.5 nm.

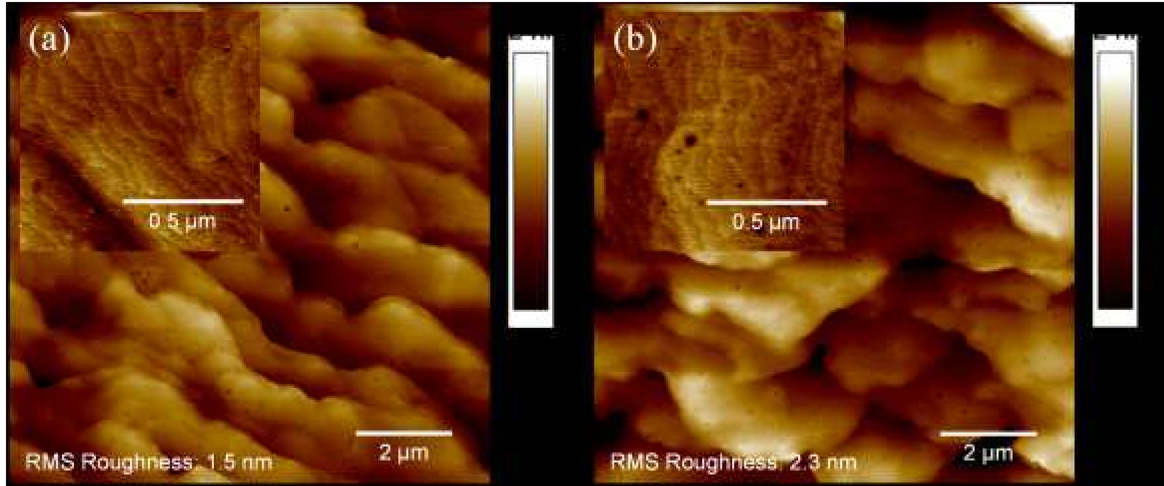

Figure 4. 10 µm × 10 µm AFM scans of (a) R0040 and (b) R0045. Insets are 1 µm × 1 µm scans with 3 nm height scale to show morphology of terraces between bunched steps. The RMS roughness of both of these scans is 0.3 nm. The step bunching observed here may be due to compressively stressed layers.

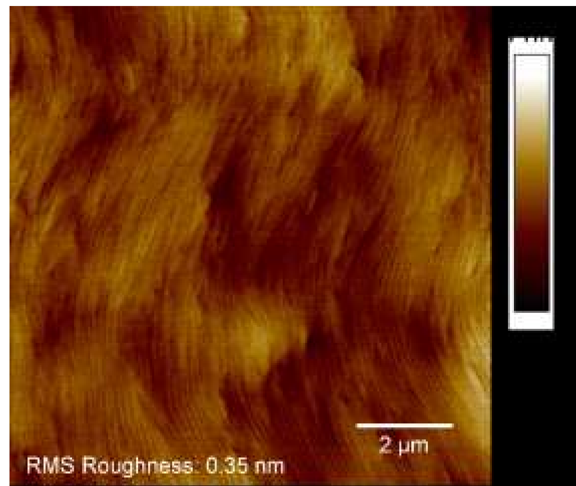

Figure 5. 10 µm × 10 µm AFM scan of R0048. Accompanying SIMS measurement showed significantly lower [Be] and more controlled Be incorporation in this sample.

X-ray rocking curve (XRC) scans were performed in both symmetric (0002) and asymmetric $(10\bar{1}2)$ planes on each sample, shown in Fig. 6, to assess crystalline quality. The full width at half maximum (FWHM) values of the symmetric XRC scans are similar for all three samples. However, the FWHM of the asymmetric XRC from R0048 is significantly smaller than the other samples. Dislocation densities were calculated to be 9.6×10^{8} cm^{-2}, 9.7×10^{8} cm^{-2}, and 4.5×10^{8} cm^{-2} for R0040, R0045, and R0048, respectively. The reduction in dislocation density by more than a factor of two for R0048 is further an indication of Be-related degradation of material quality with high dopant precursor flows. Specifically, the increase in asymmetric XRC FWHM indicates an increase in edge and mixed dislocation density associated with high [Be].

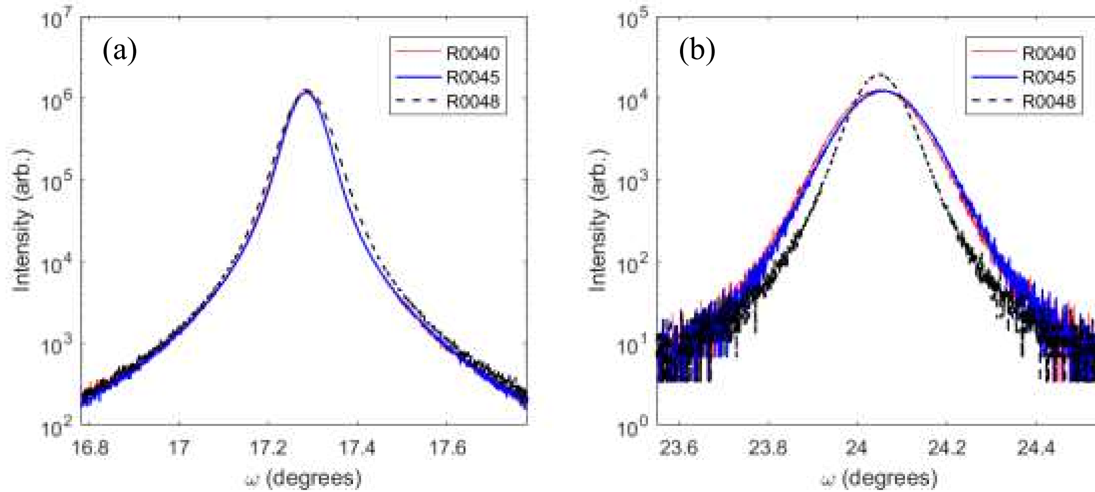

Figure 6. (a) symmetric (0002) and (b) asymmetric $(10\bar{1}2)$ x-ray rocking curve (ω) scans of GaN:Be material.

Similar results were obtained for other growth conditions shown in Table 1. At the high molar flow of Be(acac)$_2$, [Be] saturates and SIMS traces are similar. For Be(acac)$_2$ flow less than ~500 nmol/min in this experimental set, Be incorporation is controllable and varies with the flow.

Differences in growth pressure between 100 and 300 Torr appear to have little effect on Be incorporation at these growth conditions.

Although *p*-type conduction could not be established in the samples in this preliminary study, the clear Be-acceptor-related PL peaks observed for every sample indicate that MOCVD has great potential as a robust growth methodology toward achieving reliable, high conductivity *p*-GaN:Be. The growth method appears to disfavor an incorporation pathway for oxygen from the Be source material which is promising in lowering compensation.

CONCLUSION

MOCVD-grown GaN doped *in situ* with Be was systematically investigated. Growth conditions that result in stable [Be] incorporation and smooth GaN surfaces were identified and correlated to the flow of Be precursor $Be(acac)_2$. The presence of shallow Be_{Ga} acceptors was confirmed by detailed PL characterization studies. At high $Be(acac)_2$ flow, [Be] saturates, Be incorporation becomes unstable, and material surface quality degrades. Based on these results, it appears that Be behaves similarly to other common GaN dopants such as Si and Mg and segregates into Be-rich domains when the dopant concentration exceeds the solubility limit in GaN. This may contribute to self-compensation, and further study is required to optimize doping conditions and mitigate these effects.

Although samples studied here were compensated and resistive, these preliminary results demonstrate the efficacy of MOCVD as a highly promising growth method for the investigation of GaN:Be. The clear Be-related PL peaks in every sample studied indicate that this growth method shows great potential toward achieving reliable, high conductivity *p*-GaN:Be. The

growth method appears to disfavor an incorporation pathway for oxygen from the Be source material, favorable in lower compensation.

ASSOCIATED CONTENT

Supporting Information

Beryllium 2,4-Pentanedionate SDS (PDF)

AUTHOR INFORMATION

Corresponding Author

*E-mail: mcewenb@sunypoly.edu

Author Contributions

The manuscript was written through contributions of all authors. All authors have given approval to the final version of the manuscript.

Notes

The data that support the findings of this study are available from the corresponding author upon reasonable request.

ACKNOWLEDGMENT

The work outlined here was supported by the National Science Foundation (DMR-1905186, and DMR-1904861).

REFERENCES

(1) Suvarna, P.; Bulmer, J.; Leathersich, J. M.; Marini, J.; Mahaboob, I.; Hennessy, J.; Bell, L.

D.; Nikzad, S.; Shahedipour-Sandvik, F. S. Ion Implantation-Based Edge Termination to Improve III-N APD Reliability and Performance. *IEEE Photonics Technol. Lett.* **2015**, *27* (5), 498–501. https://doi.org/10.1109/LPT.2014.2382611.

(2) Marini, J.; Mahaboob, I.; Hogan, K.; Novak, S.; Bell, L. D.; Shahedipour-Sandvik, F. Mg Incorporation Efficiency in Pulsed MOCVD of N-Polar GaN:Mg. *J. Electron. Mater.* **2017**, *46* (10), 5820–5826. https://doi.org/10.1007/s11664-017-5602-x.

(3) Mahaboob, I.; Yakimov, M.; Rocco, E.; Hogan, K.; Shahedipour-Sandvik, F. Drain-Voltage-Induced Secondary Effects in AlGaN/GaN HEMTs with Integrated Body-Diode. *IEEE Trans. Electron Devices* **2020**, *67* (10), 3983–3987. https://doi.org/10.1109/TED.2020.3001920.

(4) Rocco, E.; Mahaboob, I.; Hogan, K.; Meyers, V.; McEwen, B.; Bell, L. D.; Shahedipour-Sandvik, F. Impurity Incorporation and Diffusion from Regrowth Interfaces in N-Polar GaN Photocathodes and the Impact on Quantum Efficiency. *J. Appl. Phys.* **2021**, *129* (19). https://doi.org/10.1063/5.0049344.

(5) McEwen, B.; Mahaboob, I.; Rocco, E.; Hogan, K.; Meyers, V.; Green, R.; Nouketcha, F.; Murray, T.; Kaushik, V.; Lelis, A.; Shahedipour-Sandvik, F. Investigation of the Effects of Forming Gas Annealing on Al2O3/GaN Interface. *J. Electron. Mater.* **2021**, *50* (1), 80–84. https://doi.org/10.1007/s11664-020-08532-w.

(6) Mahaboob, I.; Reinertsen, R. J.; McEwen, B.; Hogan, K.; Rocco, E.; Melendez, J. A.; Cady, N. C.; Shahedipour-Sandvik, F. Boronate Probe-Based Hydrogen Peroxide Detection with AlGaN/GaN HEMT Sensor. *Experimental Biology and Medicine*. 2021, pp 523–528. https://doi.org/10.1177/1535370220972030.

(7) Mahaboob, I.; Hogan, K.; Novak, S. W.; Shahedipour-Sandvik, F.; Tompkins, R. P.;

Lazarus, N. Influence of Mask Material on the Electrical Properties of Selective Area Epitaxy GaN Microstructures. *J. Vac. Sci. Technol. B, Nanotechnol. Microelectron. Mater. Process. Meas. Phenom.* **2018**, *36* (3), 031203. https://doi.org/10.1116/1.5026804.

(8) Mahaboob, I.; Marini, J.; Hogan, K.; Rocco, E.; Tompkins, R. P.; Lazarus, N.; Shahedipour-Sandvik, F. Selective Area Epitaxial Growth of Stretchable Geometry AlGaN-GaN Heterostructures. *J. Electron. Mater.* **2018**, *47* (11), 6625–6634. https://doi.org/10.1007/s11664-018-6576-z.

(9) Marini, J.; Mahaboob, I.; Rocco, E.; Bell, L. D.; Shahedipour-Sandvik, F. Polarization Engineered N-Polar Cs-Free GaN Photocathodes. *J. Appl. Phys.* **2018**, *124* (11). https://doi.org/10.1063/1.5029975.

(10) Hogan, K.; Tozier, S.; Rocco, E.; Mahaboob, I.; Meyers, V.; McEwen, B.; Shahedipour-Sandvik, F.; Tompkins, R.; Derenge, M.; Jones, K.; Shevelev, M.; Sklyar, V.; Lang, A.; Hart, J.; Taheri, M.; Reshchikov, M. Novel Gyrotron Beam Annealing Method for Mg-Implanted Bulk GaN. *IEEE Int. Reliab. Phys. Symp. Proc.* **2019**, *2019-March*. https://doi.org/10.1109/IRPS.2019.8720600.

(11) Mahaboob, I.; Yakimov, M.; Hogan, K.; Rocco, E.; Tozier, S.; Shahedipour-Sandvik, F. Dynamic Control of AlGaN/GaN HEMT Characteristics by Implementation of a p-GaN Body-Diode-Based Back-Gate. *IEEE J. Electron Devices Soc.* **2019**, *7* (March), 581–588. https://doi.org/10.1109/JEDS.2019.2915097.

(12) Rocco, E.; Licata, O.; Mahaboob, I.; Hogan, K.; Tozier, S.; Meyers, V.; McEwen, B.; Novak, S.; Mazumder, B.; Reshchikov, M.; Douglas Bell, L.; Shahedipour-Sandvik, F. Hillock Assisted P-Type Enhancement in N-Polar GaN:Mg Films Grown by MOCVD. *Sci. Rep.* **2020**, *10* (1), 1–8. https://doi.org/10.1038/s41598-020-58275-1.

(13) Mahaboob, I.; Novak, S. W.; Rocco, E.; Hogan, K.; Shahedipour-Sandvik, F. Investigation of the Electrical Behavior of AlGaN/GaN High Electron Mobility Transistors Grown with Underlying GaN:Mg Layer. *J. Vac. Sci. Technol. B* **2020**, *38* (6), 062204. https://doi.org/10.1116/6.0000255.

(14) Meyers, V.; Rocco, E.; Hogan, K.; Tozier, S.; McEwen, B.; Mahaboob, I.; Shahedipour-Sandvik, F. Removal of Dry-Etch-Induced Surface Layer Damage from p-GaN by Photoelectrochemical Etching. *J. Electron. Mater.* **2020**, *49* (6), 3481–3489. https://doi.org/10.1007/s11664-020-07986-2.

(15) Amano, H.; Kito, M.; Hiramatsu, K.; Akasaki, I. P-Type Conduction in Mg-Doped GaN Treated with Low-Energy Electron Beam Irradiation (LEEBI). *Jpn. J. Appl. Phys.* **1989**, *28* (12 A), L2112–L2114. https://doi.org/10.1143/JJAP.28.L2112.

(16) Pantha, B. N.; Lin, Y. J.; Jiang, H. X. High Quality Al-Rich AlGaN Alloys. In *GaN and ZnO-Based Materials and Devices*; Pearton, S.; Springer: Berlin, 2012; pp 29–81.

(17) Obloh, H.; Bachem, K. H.; Kaufmann, U.; Kunzer, M.; Maier, M.; Ramakrishnan, A.; Schlotter, P. Self-Compensation in Mg Doped p-Type GaN Grown by MOCVD. *J. Cryst. Growth* **1998**, *195* (1–4), 270–273. https://doi.org/10.1016/S0022-0248(98)00578-8.

(18) Bernardini, F.; Fiorentini, V.; Bosin, A. Theoretical Evidence for Efficient P-Type Doping of GaN Usina Beryllium. *Appl. Phys. Lett.* **1997**, *70* (22), 2990–2992. https://doi.org/10.1063/1.118766.

(19) Dewsnip, D. J.; Andrianov, A. V.; Harrison, I.; Orton, J. W.; Lacklison, D. E.; Ren, G. B.; Hooper, S. E.; Cheng, T. S.; Foxon, C. T. Photoluminescence of MBE Grown Wurtzite Be-Doped GaN. *Semicond. Sci. Technol.* **1998**, *13* (5), 500–504. https://doi.org/10.1088/0268-1242/13/5/010.

(20) Myers, T. H.; Ptak, A. J.; Wang, L.; Giles, N. C. Magnesium and Beryllium Doping During Rf-Plasma MBE Growth of GaN. In *Proceedings of the International Workshop on Nitride Semiconductors, Institute of Pure and Applied Physics Conference Series 1*; 2000; pp 451–454.

(21) Sun, Y.; Tan, L. S.; Chua, S. J.; Prakash, S. Activation of Beryllium-Implanted GaN by Two-Step Annealing. *Mater. Res. Soc. Symp. - Proc.* **2000**, *595*. https://doi.org/10.1557/proc-595-f99w3.82.

(22) Katzer, D. S.; Storm, D. F.; Binari, S. C.; Roussos, J. A.; Shanabrook, B. V.; Glaser, E. R. Molecular Beam Epitaxy of Beryllium-Doped GaN Buffer Layers for AlGaN/GaN HEMTs. *MBE 2002 - 2002 12th Int. Conf. Mol. Beam Ep.* **2002**, *251*, 233–234. https://doi.org/10.1109/MBE.2002.1037845.

(23) Storm, D. F.; Katzer, D. S.; Deen, D. A.; Bass, R.; Meyer, D. J.; Roussos, J. A.; Binari, S. C.; Paskova, T.; Preble, E. A.; Evans, K. R. Proximity Effects of Beryllium-Doped GaN Buffer Layers on the Electronic Properties of Epitaxial AlGaN/GaN Heterostructures. *Solid. State. Electron.* **2010**, *54* (11), 1470–1473. https://doi.org/10.1016/j.sse.2010.05.041.

(24) Teisseyre, H.; Bockowski, M.; Grzegory, I.; Kozanecki, A.; Damilano, B.; Zhydachevskii, Y.; Kunzer, M.; Holc, K.; Schwarz, U. T. GaN Doped with Beryllium - An Effective Light Converter for White Light Emitting Diodes. *Appl. Phys. Lett.* **2013**, *103* (1). https://doi.org/10.1063/1.4812335.

(25) Ahmad, H.; Lindemuth, J.; Engel, Z.; Matthews, C. M.; McCrone, T. M.; Doolittle, W. A. Substantial P-Type Conductivity of AlN Achieved via Beryllium Doping. *Adv. Mater.* **2021**, *33* (42). https://doi.org/10.1002/adma.202104497.

(26) Lany, S.; Zunger, A. Dual Nature of Acceptors in GaN and ZnO: The Curious Case of the

Shallow Mg_{Ga} Deep State. *Appl. Phys. Lett.* **2010**, *96* (14). https://doi.org/10.1063/1.3383236.

(27) Lyons, J. L.; Janotti, A.; Van De Walle, C. G. Impact of Group-II Acceptors on the Electrical and Optical Properties of GaN. *Jpn. J. Appl. Phys.* **2013**, *52* (8 PART 2). https://doi.org/10.7567/JJAP.52.08JJ04.

(28) Cai, X.; Yang, J.; Zhang, P.; Wei, S. H. Origin of Deep Be Acceptor Levels in Nitride Semiconductors: The Roles of Chemical and Strain Effects. *Phys. Rev. Appl.* **2019**, *11* (3), 1–7. https://doi.org/10.1103/PhysRevApplied.11.034019.

(29) Demchenko, D. O.; Vorobiov, M.; Andrieiev, O.; Myers, T. H.; Reshchikov, M. A. Shallow and Deep States of Beryllium Acceptor in GaN: Why Photoluminescence Experiments Do Not Reveal Small Polarons for Defects in Semiconductors. *Phys. Rev. Lett.* **2021**, *126* (2), 27401. https://doi.org/10.1103/PhysRevLett.126.027401.

(30) Al Tahtamouni, T. M.; Sedhain, A.; Lin, J. Y.; Jiang, H. X. Beryllium Doped P-Type GaN Grown by Metal- Organic Chemical Vapor Deposition. *Jordan J. Phys.* **2010**, *3* (2), 77–81.

(31) Truemper, J. T. A Study of the Volatile Characteristics of Various Metal β-Diketone Chelate Compounds, 1959, Vol. 571. https://doi.org/10.1021/j100833a029.

(32) Reshchikov, M. A. Measurement and Analysis of Photoluminescence in GaN. *J. Appl. Phys.* **2021**, *129* (12). https://doi.org/10.1063/5.0041608.

(33) Reshchikov, M. A.; Vorobiov, M.; Demchenko, D. O.; Ozgur; Morkoç, H.; Lesnik, A.; Hoffmann, M. P.; Hörich, F.; Dadgar, A.; Strittmatter, A. Two Charge States of the C N Acceptor in GaN: Evidence from Photoluminescence. *Phys. Rev. B* **2018**, *98* (12), 125207. https://doi.org/10.1103/PhysRevB.98.125207.

(34) Vorobiov, M.; Andrieiev, O.; Demchenko, D. O.; Reshchikov, M. A. Point Defects in

Beryllium-Doped GaN. *Phys. Rev. B* **2021**, *104* (24), 245203. https://doi.org/10.1103/PhysRevB.104.245203.

(35) Reshchikov, M. A.; Kvasov, A. A.; Bishop, M. F.; McMullen, T.; Usikov, A.; Soukhoveev, V.; Dmitriev, V. A. Tunable and Abrupt Thermal Quenching of Photoluminescence in High-Resistivity Zn-Doped GaN. *Phys. Rev. B - Condens. Matter Mater. Phys.* **2011**, *84* (7), 1–22. https://doi.org/10.1103/PhysRevB.84.075212.

(36) Ptak, A. J.; Myers, T. H.; Wang, L.; Giles, N. C.; Maldovan, M.; Da Cunha, C. R.; Hornak, L. A.; Tian, C.; Hockett, R. A.; Mitha, S.; Van Lierde, P. A Comparison of Magnesium and Beryllium Acceptors in GaN Grown by Rf-Plasma Assisted Molecular Beam Epitaxy. *Mater. Res. Soc. Symp. - Proc.* **2001**, *639*, G3.3.1-G3.3.6. https://doi.org/10.1557/proc-639-g3.3.

(37) Ptak, A. J.; Wang, L.; Giles, N. C.; Myers, T. H.; Romano, L. T.; Tian, C.; Hockett, R. A.; Mitha, S.; Van Lierde, P. Incorporation-Related Structural Issues for Beryllium Doping during Growth of GaN by Rf-Plasma Molecular-Beam Epitaxy. *Appl. Phys. Lett.* **2001**, *79* (27), 4524–4526. https://doi.org/10.1063/1.1429290.

(38) Figge, S.; Kröger, R.; Böttcher, T.; Ryder, P. L.; Hommel, D. Magnesium Segregation and the Formation of Pyramidal Defects in P-GaN. *Appl. Phys. Lett.* **2003**, *81* (25), 4748–4750. https://doi.org/10.1063/1.1527981.

(39) Hashizume, T. Effects of Mg Accumulation on Chemical and Electronic Properties of Mg-Doped p-Type GaN Surface. *J. Appl. Phys.* **2003**, *94* (1), 431–436. https://doi.org/10.1063/1.1580195.

(40) Schmidt, T.; Siebert, M.; Flege, J. I.; Gangopadhyay, S.; Pretorius, A.; Kröger, R.; Figge, S.; Gregoratti, L.; Barinov, A.; Hommel, D.; Falta, J. Surface Segregation of Si and Mg

Dopants in MOVPE Grown GaN Films Revealed by X-Ray Photoemission Spectro-Microscopy. *Phys. Status Solidi Curr. Top. Solid State Phys.* **2006**, *3* (6), 1725–1728. https://doi.org/10.1002/pssc.200565437.

(41) Schmidt, T. H.; Siebert, M.; Flege, J. I.; Figge, S.; Gangopadhyay, S.; Pretorius, A.; Lee, T. L.; Zegenhagen, J.; Gregoratti, L.; Barinov, A.; Rosenauer, A.; Hommel, D.; Falta, J. Mg and Si Dopant Incorporation and Segregation in Gan. *Phys. Status Solidi Basic Res.* **2011**, *248* (8), 1810–1821. https://doi.org/10.1002/pssb.201046531.

(42) Sun, Q.; Selloni, A.; Myers, T. H.; Doolittle, W. A. Energetics of Mg Incorporation at GaN(0001) and GaN (000 $\bar{1}$) Surfaces. *Phys. Rev. B - Condens. Matter Mater. Phys.* **2006**, *73* (15), 1–9. https://doi.org/10.1103/PhysRevB.73.155337.

(43) Northrup, J. E. Hydrogen and Magnesium Incorporation on c -Plane and m -Plane GaN Surfaces. *Phys. Rev. B - Condens. Matter Mater. Phys.* **2008**, *77* (4), 1–7. https://doi.org/10.1103/PhysRevB.77.045313.

(44) Bennett, S. E.; Ulfig, R. M.; Clifton, P. H.; Kappers, M. J.; Barnard, J. S.; Humphreys, C. J.; Oliver, R. A. Atom Probe Tomography and Transmission Electron Microscopy of a Mg-Doped AlGaN/GaN Superlattice. *Ultramicroscopy* **2011**, *111* (3), 207–211. https://doi.org/10.1016/j.ultramic.2010.11.028.

(45) Khromov, S.; Gregorius, D.; Schiller, R.; Lösch, J.; Wahl, M.; Kopnarski, M.; Amano, H.; Monemar, B.; Hultman, L.; Pozina, G. Atom Probe Tomography Study of Mg-Doped GaN Layers. *Nanotechnology* **2014**, *25* (27). https://doi.org/10.1088/0957-4484/25/27/275701.

(46) Wang, H.; Liu, J.; Niu, N.; Shen, G.; Zhang, S. Enhanced Performance of P-GaN by Mg δ Doping. *J. Cryst. Growth* **2007**, *304* (1), 7–10. https://doi.org/10.1016/j.jcrysgro.2007.01.040.

(47) Northrup, J. E. Incorporation of Beryllium on the Clean and Indium-Terminated GaN(0001) Surface. *Appl. Phys. Lett.* **2001**, *78* (19), 2855–2857. https://doi.org/10.1063/1.1368369.

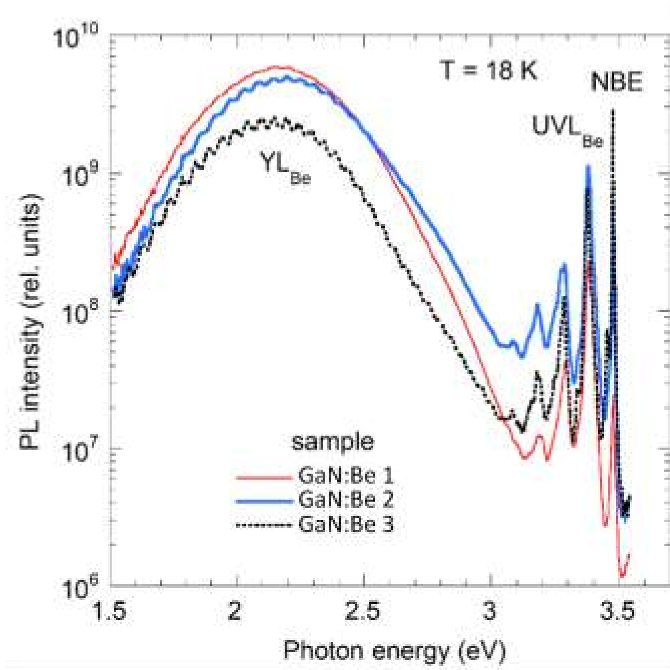

For Table of Contents Only